Inelastic neutron scattering of lithium tantalate studied in the ferroelectric and paraelectric phases

1993 J. Phys.: Condens. Matter 5 2707

(http://iopscience.iop.org/0953-8984/5/17/005)

J. Phys.: Condens. Matter 5 (1993) 2707–2718. Printed in the UK

Inelastic neutron scattering of lithium tantalate studied in the ferroelectric and paraelectric phases

Gou Cheng†, B Hennion‡, P Launois‡, Meng Xianlin§, Xu Binchao§ and Jiang Yimin†

† Institute of Atomic Energy, PO Box 275, Beijing, People's Republic of China
‡ Laboratoire Léon Brillouin, 91191 Saclay Cédex, France
§ Institute of Crystal Materials, Shandong University, Jinan, People's Republic of China

Received 23 November 1992

Abstract. Inelastic neutron scattering measurements on single-crystal $LiTaO_3$ in the temperature range from room temperature to 800 °C show evidence of overdamped scattering, both below and above the ferroelectric-to-paraelectric phase transition. The results are qualitatively discussed in comparison with the recent Raman studies. The measurements failed to observe any well defined underdamped soft mode in the experimental setting that favours detection of the ferroelectric mode (the lowest-frequency A_1(TO) mode), thereby not supporting a conventional displacive picture of phase transition in the crystal. We also measured some low-frequency phonon dispersions along two symmetry directions at room temperature.

1. Introduction

Lithium tantalate ($LiTaO_3$) and the isomorphic lithium niobate ($LiNbO_3$) are uniaxial ferroelectrics with a single phase transition of second order. Their dynamical properties near the Curie temperatures have been the subject of considerable interest over the last two decades. Although a large number of spectroscopic studies, including Raman [1–3], infrared, nuclear magnetic resonance (NMR), and Mössbauer spectroscopies [4] have been made over a wider range of temperatures, a proper picture of the dynamics close to the ferroelectric-to-paraelectric transition temperature at the microscopic level remains obscure. In recent publications, there is a common tendency to adopt the idea that the order–disorder mechanism is responsible in the transition region for both materials [4, 5]. Furthermore, the dynamical behaviours of these compounds are shown to be strongly coupled with the defects in the crystal as many physical properties differ depending on the method used to prepare the samples and the deviation from stoichiometry [6].

In recent Raman studies [1, 3], intense quasi-elastic scattering is observed in the zz-polarizability tensor component. The central component broadens with increasing temperature up to about 750 K and then narrows as the temperature increases further. At about 750 K, the broad structure may extend up to about 250 cm^{-1}. Moreover, the Raman spectra indicate that the lowest A_1(TO) mode at 203 cm^{-1} undergoes strong damping above 550 K, and its peak becomes unclear because of the broadening of the central component and the appearance of other bands in the region. A main purpose of the present paper is to use the inelastic neutron scattering method to investigate the notable features observed in the Raman spectra. As is well known, neutron scattering admits both energy and lattice

momentum transfers between the incident beam and target crystal, so that we can study the central component in both E (energy) and q (momentum) spaces.

Many spectroscopic studies of $LiTaO_3$ or $LiNbO_3$ were stimulated by the long-time controversy concerning whether their ferroelectric phase transition is either displacive or order–disorder in character. One could find an illustration of these two alternative descriptions in the recent work of Birnie [5]. The Raman spectroscopy studies reported by different workers are quite contradictory. Some studies support the displacive model [7], while others support the order–disorder model [1–3, 8]. In such a situation, the data from inelastic neutron scattering will be of particular interest for obtaining a correct picture of phase transition. We note that early work on elastic neutron scattering by Samuelsen and Grande [9] gives strong evidence in favour of the order–disorder model for $LiTaO_3$.

In our work we shall investigate the inelastic neutron spectra of $LiTaO_3$ at both room temperature and high temperatures. The results are qualitatively discussed in comparison with Raman studies and other neutron investigations performed on other ferroelectrics. We also present measurements for acoustic phonon dispersions and an optical phonon branch along two symmetry directions in the Brillouin zone at room temperature.

2. Experimental details

2.1. Sample preparation

Natural Li metal is a mixture of the two isotopes ^6Li (7.4%) and ^7Li (92.6%). Since ^6Li is a heavy absorber of thermal neutrons ($\sigma_a = 945$ b for 1.8 Å neutrons), samples with a separated ^7Li isotope are preferable for the present measurements. For this purpose, $^7Li_2CO_3$ was made and was mixed with Ta_2O_5 and heated to about 1700 °C. A large single crystal of very good quality was then pulled from the melt by the Czochralski method at the Institute of Crystal Materials, Shandong University. A sample was prepared that has the congruent-melting composition, which is about 4.9% deficient in Li. The crystal was of cylindrical shape of diameter 2 cm and height 4 cm, the cylindrical axis being a hexagonal a axis (i.e. along $\langle 010 \rangle$).

As is known, some physical properties of the $LiTaO_3$ crystal may differ depending on the way that the crystal is prepared [6]. Giving some sample specifications is therefore useful. For our sample, the room-temperature lattice parameters obtained by x-ray scattering are $a = 5.153$ Å and $c = 13.775$ Å. The ferroelectric-to-paraelectric transition temperature T_c determined from the dielectric measurements is 893 ± 10 K. T_c can be obtained also by observing the temperature dependence of the diffraction intensity of the $(\bar{2}\,0\,10)$ reflection. Such a measurement was performed for the sample and is shown in figure 1. It gives $T_c \simeq 890$ K, which is in good agreement with the T_c obtained from the dielectric measurements.

2.2. Neutron measurements

The neutron measurements were performed on the 1T1 and G4-3 instruments at the ORPHEE reactor of Laboratoire Léon Brillouin, Saclay. The monochromator used is pyrolytic graphite with a pyrolytic graphite filter. The incident neutron wavenumber is 2.662 $Å^{-1}$. For high-temperature measurements, the sample was mounted in a closed furnace and kept in vacuum while the temperature was raised to about 1100 K. No evidence of oxidation was observed on the sample surface layers after the experiments. Both constant-Q and constant-ΔE techniques were employed in the measurements.

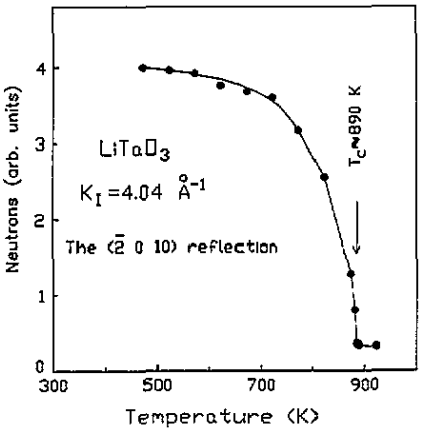

Figure 1. Neutron intensities of the $(\bar{2}\,0\,10)$ reflection versus temperature.

The $LiTaO_3$ lattice belongs to the rhombohedral system of axes with the $R3c$ and $R\bar{3}c$ space groups at temperatures below and above, respectively, the transition temperature. Because it is isostructural with $LiNbO_3$, the group theory and neutron selection rules for $LiNbO_3$ in [10, 11] could be directly used in the planning of the present experiments. With the $R3c$ space group, there are two directions in the lattice that are considered interesting from the symmetry point of view. One is along the threefold axis, being denoted by Λ. The other is in one of the glide planes and perpendicular to the threefold axis. This direction is denoted by Σ.

The ten atoms per primitive unit cell of $LiTaO_3$ will give 30 branches of dispersion curves. For q along the Λ direction, the symmetry classification of the branches is $5\Lambda_1+5\Lambda_2+10\Lambda_3$, where Λ_1 and Λ_2 are one-dimensional irreducible representations of the point group of the wavevector q and Λ_3 is a two-dimensional representation. By selecting experimental conditions, we can completely separate the three types of branch. In particular, with the scattering vector Q parallel to the threefold axis, the Λ_3 modes are not neutron active; Λ_1 and Λ_2 can be measured in even and odd Brillouin zones, respectively. Once the Λ_1 and Λ_2 modes have been established, there should be no difficulty in identifying the Λ_3 modes by setting Q nearly perpendicular to the threefold axis. For q along the Σ direction, the classification is $15\Sigma_1 + 15\Sigma_2$ with Σ_1 and Σ_2 one-dimensional irreducible representations. No selection rules exist in this direction such that one or the other of the Σ_1 and Σ_2 symmetry branches could be observed exclusively. So, the symmetry types of phonon branch can only be estimated from the compatibility relations between the Γ point, the Λ direction and the Σ direction. Theoretical calculations based on some phenomenological models are also helpful for identifying the symmetry types.

For the purpose of the present paper, we use the hexagonal system of notation for the rhombohedral $LiTaO_3$ lattice. The hexagonal c axis is along the threefold axis and the a axis perpendicular to a glide plane. The phonon dispersions along the Λ and Σ directions were obtained at room temperature. The measurements at elevated temperatures were mainly planned to study the possible quasi-elastic scattering, phonon softening and damping associated with the structure phase transition. Therefore, they were carried out in the low-energy region and near the centre of the Brillouin zone. All measurements were made around a number of reciprocal-lattice points, including the (0, 0, 6), (0, 0, 12)

and (0, 3, 0) points. These will allow us to have both longitudinal setting and transverse or nearly transverse setting during the dispersion measurements along both Λ and Σ directions.

3. Results and discussion

3.1. Phonon dispersions

Of the large number of phonon branches, the present work will not concentrate on the determination of the optical branches. Thus, our measurements here will be limited to the acoustic branches. However, an optical branch which, according to the displacive transition interpretation, is expected to be associated with the paraelectric-to-ferroelectric transition is also measured.

For phonon dispersions along the Λ direction, the longitudinal acoustic (LA) branch is measured at (0, 0, 6) or (0, 0, 12) reciprocal-lattice points, while the transverse acoustic (TA) branch is measured at the (0, 3, 0) point. Figure 2 shows the two measured branches. Figure 3 gives two typical scattered neutron profiles for two Λ acoustic phonons, one being in the constant-ΔE scan and the other in the constant-Q scan.

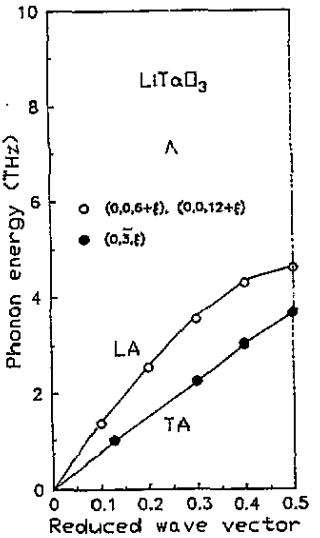

Figure 2. The measured phonon dispersion curves along the Λ direction at room temperature. The lines drawn through the experimental points are intended only as a guide to the eye.

The LA branch along the Σ direction could be easily obtained by setting $Q = (0, 3+\xi, 0)$, where ξ varies from zero to the value corresponding to the zone boundary (0.55). Another acoustic branch transversely polarized can be measured by taking $Q = (0, \xi, 6)$ or $(0, \xi, 12)$. Note that the terms 'transverse' and 'longitudinal' here mean only that the branches become purely transverse (polarization $e \perp q$) or longitudinal ($e \parallel q$) as q approaches the zone centre. There is still a third acoustic branch, as identified from the $Q = (\xi, 3, 0)$ setting. These three acoustic branches are illustrated in figure 4.

The symmetries of these acoustic branches could be determined using the compatibility relations between the Γ point and Σ direction, together with the information available from

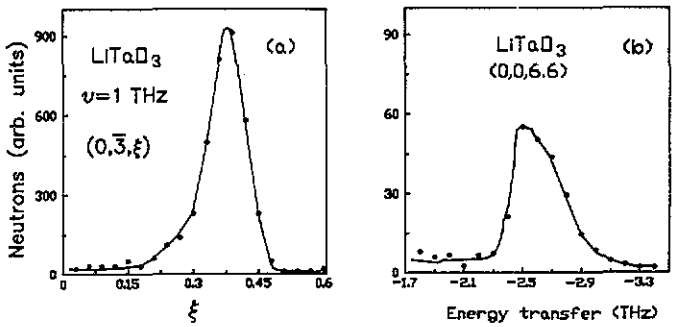

Figure 3. (*a*) Constant-ΔE scan in a transverse experimental geometry, showing a Λ_3 acoustic phonon; (*b*) constant-Q scan at $(0, 0, 6.6)$, showing the energy profile for a Λ_1 phonon. The curves drawn through the measured points are intended only as a guide to the eye.

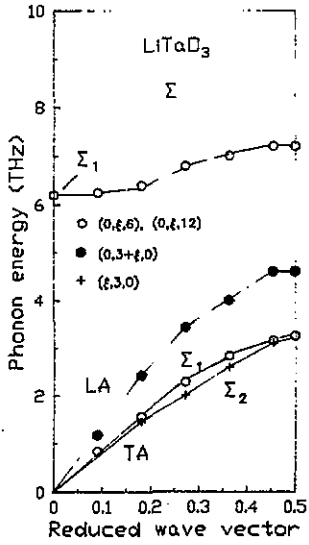

Figure 4. The measured phonon dispersion curves along the Σ direction at room temperature. The lines drawn through the experimental points are intended only as a guide to the eye.

the experimental setting. As the wavevector $q \to 0$, the LA branch with Σ_1 symmetry is polarized on the glide reflection plane and perpendicular to the threefold axis. This is sufficient to conclude that the branch measured by the $Q = (0, 3 + \xi, 0)$ setting is of Σ_1 symmetry. Another acoustic branch with Σ_1 symmetry is transversely polarized in the $q \to 0$ limit. The branch is compatible with the Λ_1 symmetry at $q \simeq 0$ with the result that it is polarized along the threefold axis. Thus, the data collected around the $(0, 0, 6)$ and $(0, 0, 12)$ reciprocal-lattice points too are of Σ_1 symmetry. Both the Σ_1(LA) and the Σ_2(TA) modes have a finite cross section in the $Q = (\xi, 3, 0)$ setting, because here the angle between q and Q is $\pi/6$. However, since the Σ_1(LA) branch is obviously higher than the Σ_2(TA) branch, our measured phonon peaks with the lowest energy in this experimental position must be of Σ_2 symmetry. Figure 5 shows four energy profiles for two Σ_1 and two Σ_2 phonons. It is interesting to note that the Σ_1(TA) branch is very close to the Σ_2(TA)

branch. As illustrated in figure 5, the small difference between them is observable within the present experimental resolution. A comparison between the measured acoustic branches and those computed from a rigid-ion model calculation [12] is given in figure 6. It can be seen that the agreement is quite good.

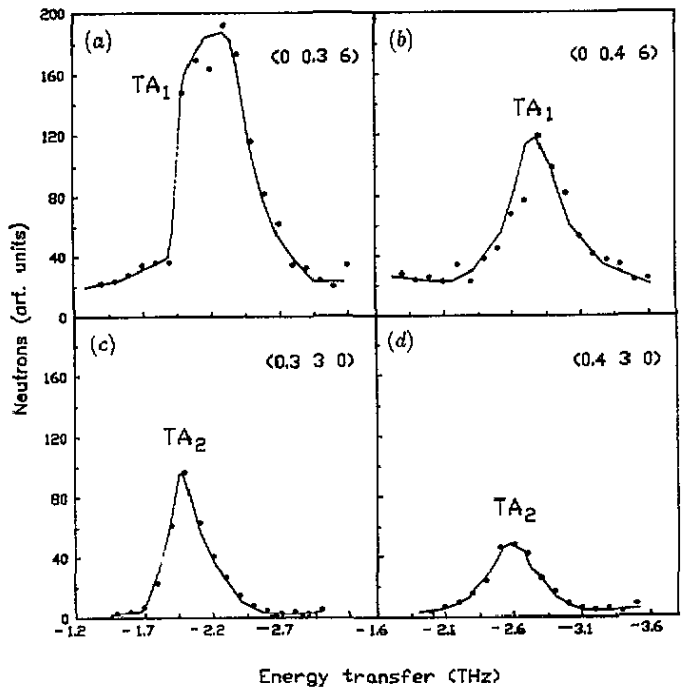

Figure 5. (*a*), (*b*) Constant-Q scans at (*a*) (0, 0.3, 6) and (*b*) (0, 0.4, 6), showing two Σ_1 acoustic phonons. (*c*), (*d*) Constant-Q scans at (*c*) (0.3, 3, 0) and (*d*) (0.4, 3, 0), showing two Σ_2 acoustic phonons.

The presence of a large number of optical modes and the lack of any useful selection rules along the Σ direction will make the dispersion measurements very difficult. In the present work we shall not try to disentangle these phonons and our interest will be limited only to a branch that is compatible with the lowest A_1(TO)mode at $q \simeq 0$. The mode has received much attention in Raman spectroscopy studies because of its notable temperature effect. In figure 7, we show six energy profiles measured in the $Q = (0, \xi, 6)$ experimental geometry, with a scattered neutron energy gain from 1 to 9 THz. The branch occurs near 6.5 THz with a small dispersion and has a relatively large intensity in this experimental position throughout the entire dispersion curve. By invoking the compatibility relations and the experimental information we can conclude that the branch at $q \simeq 0$ is really of A_1 symmetry. However, it is still insufficient to state that it is a Σ_1 branch compatible with the lowest A_1 optical mode at $q \simeq 0$ since, for general q apart from 0, there are several neighbouring branches which may also have finite cross sections (see figure 6) and it is possible that the optical dispersion in figure 4 represents a phonon band rather than a single dispersion curve. The neutron-measured A_1(TO) mode frequency is, as estimated from the $Q = (0, 0.1, 6)$ profile (figure 7), about 6.15 THz, i.e. in good agreement with the Raman spectroscopy value of 6.08 THz (203 cm^{-1}) [1]. It is worth mentioning that, because of the finite resolution in Q-space, the phonon peak at the reciprocal-lattice point (0, 0, 6) may

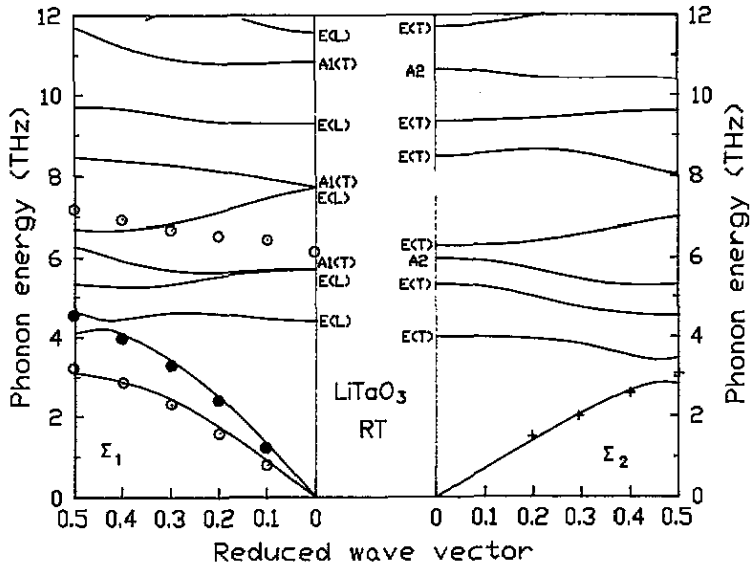

Figure 6. Comparison between the experimental points and theory along the Σ direction. The full curves are computed from a rigid-ion model [12].

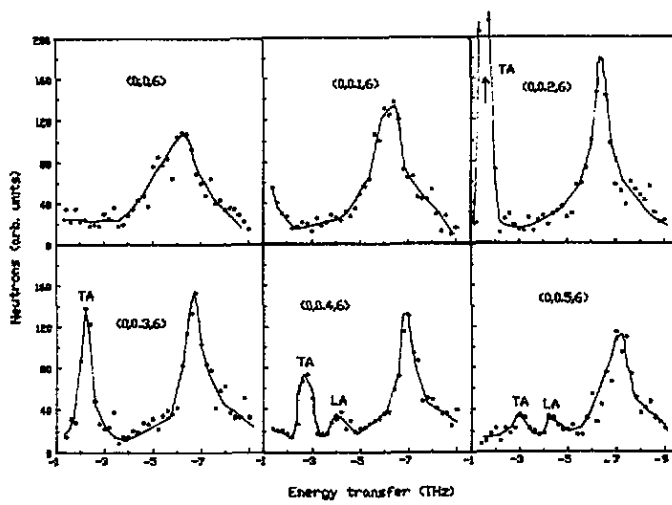

Figure 7. Constant-Q scan along the Σ direction in longitudinal experimental position at room temperature, showing an optical branch near 7 THz. The curves drawn through the measured points are intended only as a guide to the eye.

consist of many unresolved peaks including both transverse and longitudinal modes. So, a relatively broad structure appeared in the profile.

To our knowledge, the present neutron measurements of phonon dispersions for $LiTaO_3$ are the first published in the literature. A comparison between the acoustic curves of $LiTaO_3$ and those of $LiNbO_3$ [10] shows that the former is about 30–40% lower than the latter. This difference could be understood predominantly as a result of the difference between the Ta and Nb masses.

3.2. Scattering at elevated temperatures

$LiTaO_3$ is a uniaxial ferroelectric compound. According to the displacive transition interpretation, the phonon mode which is expected to be associated with the paraelectric-to-ferroelectric transition is an optical mode of A_{2u} symmetry in the paraelectric phase that will be reduced to an optical mode of $\Gamma_1(A_1)$ symmetry in the ferroelectric phase. To investigate the spectral response of the ferroelectric fluctuations, the primary set of neutron data were collected around the (0, 0, 6) reciprocal-lattice points in a transverse experiment position (i.e. q along the (1, 0, 0) direction). The experimental results are shown in figure 8. Note that the strong increase in the neutron intensity in figure 8(a) which starts at about 1 THz is interpreted as coming from the scattering of $q \simeq 0$ acoustic phonons, caused by the finite Q-resolution of the instruments. On heating, the neutron spectra in figure 8 exhibit a strongly damped phonon mode that quickly becomes overdamped at about 500 °C. This is qualitatively in agreement with Raman observations, which have concluded that there are damping and overdamping of the lowest A_1(TO) mode [1, 3]. Unfortunately, because of the weak neutron intensity of the lowest A_1(TO) phonon peak, we could not definitely draw the conclusion that the overdamped scattering is really given by the phonon mode. Because of the weakness of the phonon peak and the intervention of the $q \simeq 0$ acoustic mode and another quasi-elastic scattering mode (to be discussed below), we shall not make any quantitative fitting of the neutron spectra using a phenomenological formula for the susceptibility $\chi(\omega, T)$. From figure 8, it can be seen that the overdamped scattering is presented in a large range of temperatures across the ferroelectric and paraelectric phases, namely from about 100 °C below T_c up to 800 °C. This is at variance with the Raman results, where the central component and its broad tail drop rapidly when the sample becomes paraelectric.

The q-dependence of the scattering can be sketched from figure 9. The figure shows two constant-ΔE scans along the Λ and Σ symmetry directions. It can be seen that the scattering is centred at the Brillouin zone centre and decreases rapidly when q increases. No obvious anisotropy in q is observed in figure 9. However, it has been observed that the scattering is anisotropic in the total neutron momentum transfer Q, and the greatest intensity is found when Q is nearly parallel to the ferroelectric axis of the crystal.

The quasi-elastic scattering near the zone centre and T_c is rather complicated and contains several contributions from the $q \simeq 0$ acoustic phonons, the overdamped mode, etc. Figure 10 shows the temperature dependence of the elastic cross section at two q-values near the reciprocal lattice point (0,0,6). A strong increase in the neutron intensity is observed in the phase transition region. It is reasonable to consider that the temperature effect arises predominantly from the overdamped scattering. Note that, although the elastic intensity drops to its original level at 800 °C, its high-energy part remains at a high level (see figure 8). This property seems to suggest that similar overdamped scattering exists both below and above the temperature of the phase transition. This differs from the Raman results in which the overdamped scattering was observed only for temperatures below T_c [1, 3].

The most puzzling feature in the neutron spectra of $LiTaO_3$ is the quasi-elastic scattering observed in the vicinity of the Brillouin zone centre. This could be seen if we shift the acoustic phonon peaks out of the quasi-elastic region by increasing q (figure 11). As q increases, the intensity of the quasi-elastic scattering decreases rapidly to the usual elastic incoherent background (figure 12). The component is presented at all temperatures of the experiment, and its intensity and width exhibit only slight changes with temperature. Consequently, it is less related to the phase transition. Apparently similar scattering has

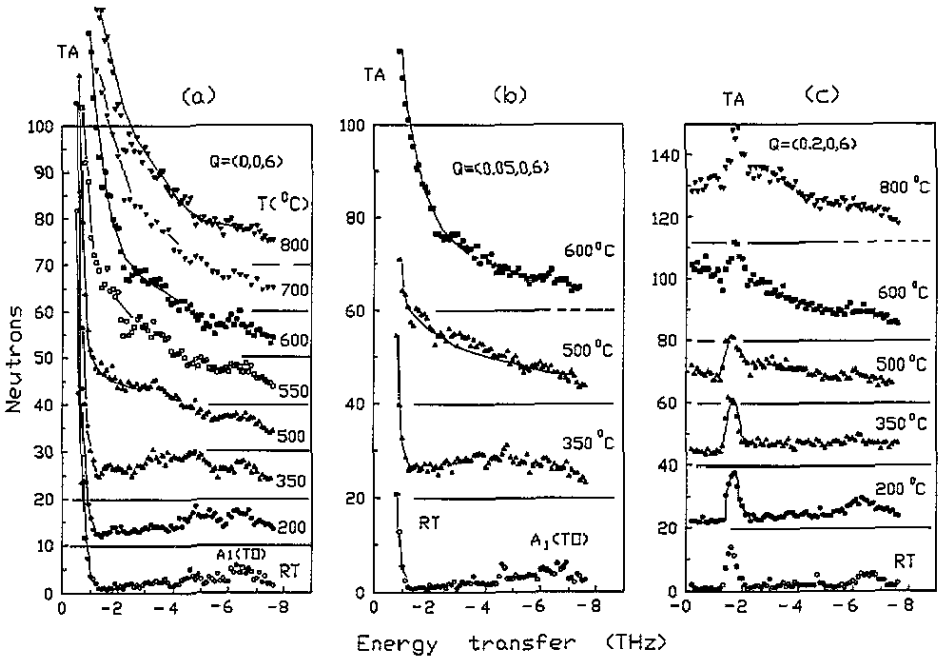

Figure 8. The neutron scattering spectra of $LiTaO_3$ at a variety of temperatures above and below T_c. The scattering wavevector $\mathbf{Q}$ is (*a*) (0, 0, 6), (*b*) (0.05, 0, 6) and (*c*) (0.2, 0, 6). The high-temperature spectra are vertically shifted for clarity. The horizontal lines are zero positions of the shifted spectra.

also been observed in other ferroelectrics, as in perovskites $KTaO_3$ [13] and $KNbO_3$ [14]. The fact that it extends to the paraelectric phase suggests that it cannot be explained by scattering on domain walls. It probably originated from the defects in the $LiTaO_3$ crystal. Further measurements on samples with different defect concentrations are needed to explore the possibility.

4. Summary and conclusion

In this work, the acoustic phonon dispersion along the Λ and Σ directions and one transverse optical phonon branch along the Σ direction of $LiTaO_3$ are measured at room temperature. These neutron scattering data, together with those of light scattering experiments, have been used in establishing a simple lattice dynamical model of the crystal [12].

Many spectroscopic measurements were made on analysing temperature effects of the neutron scattering in the phase transition region. The transverse phonon group along the Σ direction was found to have a weak intensity at room temperature. We failed to measure the temperature evolution of these phonon intensities, since they are rapidly redistributed into a rather uniform background as the temperature increases. Because no well defined underdamped soft mode was observed for the ferroelectric and paraelectric phases, the results did not support the usual displacive picture of phase transition. In the transition region, both below and above T_c, the neutron spectra show evidence of overdamped scattering. A qualitatively similar feature was also seen in the recent Raman spectra in the ferroelectric

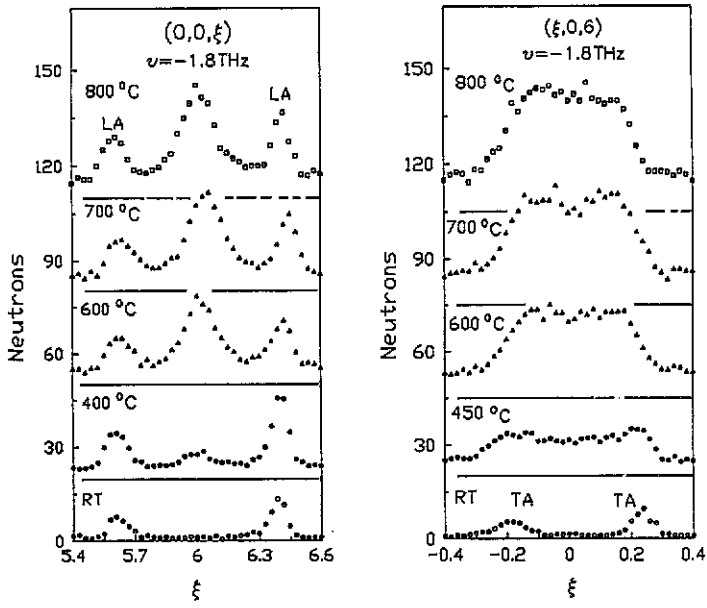

Figure 9. Neutron intensities of constant-ΔE scan along the Λ and Σ directions in a longitudinal experiment position at various temperatures. The spectra are vertically shifted for clarity; the horizontal lines indicate their zero positions.

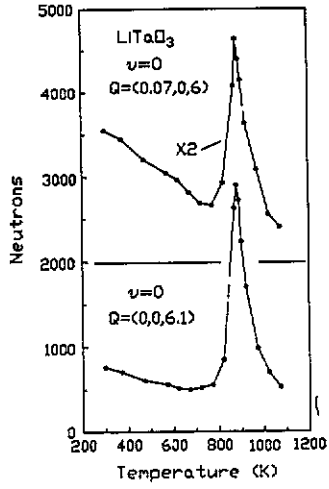

Figure 10. The intensities of two elastic neutron scatterings in $LiTaO_3$, as functions of temperature. The scattering wavevectors are at (0, 0, 6.1) and (0.07, 0, 6), respectively. The horizontal line refers to the zero position of the vertically shifted (upper) curve.

phase, but not in the paraelectric phase. We suggest that some low optical mode of A_{2u} symmetry in the paraelectric phase which is reduced to an optical mode of A_1 symmetry in the ferroelectric phase becomes overdamped in the transition region.

In the vicinity of the Brillouin zone centre, we observed unexpected quasi-elastic scattering, the intensity of which is almost independent of temperature. The origin of the

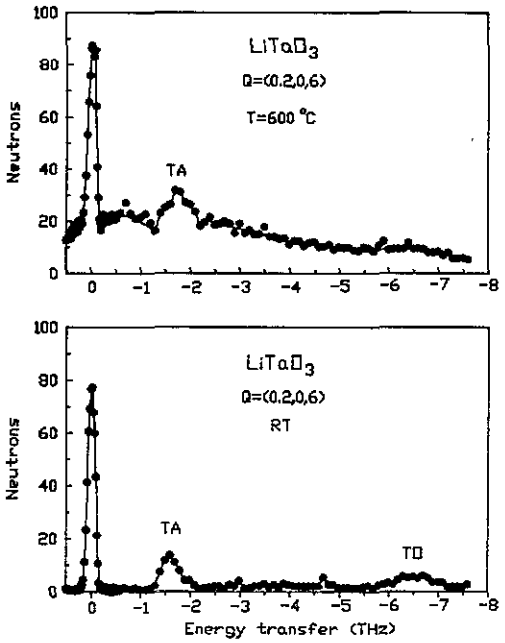

Figure 11. The neutron scattering spectra of $LiTaO_3$ for $Q = (0.2, 0, 6)$ at $T = 600\,^{\circ}C$ and room temperature.

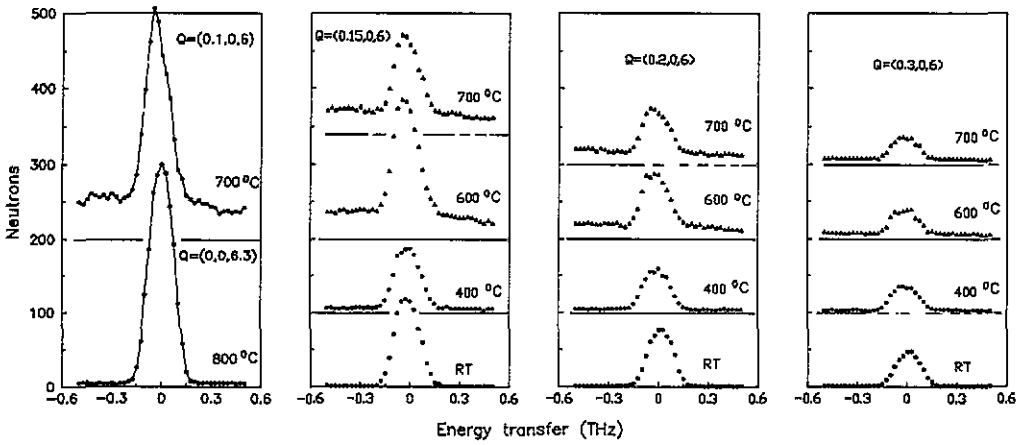

Figure 12. Energy profiles of the central component at various temperatures and the scattering wavevectors indicated in the figure. The neutron spectra are vertically shifted for clarity with their zero positions shown by the horizontal lines.

scattering is still a problem to us. We shall just mention that apparently similar scattering modes were reported in early neutron studies of the perovskites $KTaO_3$, $KNbO_3$, $KMnF_3$ and $SrTiO_3$.

References

[1] Zhang M and Scott J F 1986 *Phys. Rev.* B **34** 1880
[2] Okamoto Y, Wang P and Scott J F 1985 *Phys. Rev.* B **32** 6787
[3] Raptis C 1988 *Phys. Rev.* B **38** 10007
[4] Catchen G L and Spaar D M 1991 *Phys. Rev.* B **44** 12137
[5] Birnie D P III 1990 *J. Mater. Res.* **5** 1933; 1991 *J. Am. Ceram. Soc.* **74** 988
[6] Barns R L and Carruthers J R 1970 *J. Appl. Crystallogr.* **3** 395
[7] Johnston W D and Kaminow I P 1968 *Phys. Rev.* **68** 1045
Servoin J L and Gervais F 1979 *Solid State Commun.* **31** 387; 1980 *Ferroelectrics* **25** 609
[8] Ivanova S V, Gorelik V S and Strukov B A 1978 *Ferroelectrics* **21** 563
Jayaraman A and Ballman A A 1986 *J. Appl. Phys.* **60** 1208
Penna A F, Chaves A and Porto S P S 1976 *Solid State Commun.* **19** 491
[9] Samuelsen E J and Grande A P 1976 *Z. Phys.* B **24** 207
[10] Chowdhury M R, Peckham G E and Saunderson D H 1978 *J. Phys. C: Solid State Phys.* **11** 1671
[11] Davine S and Peckham G 1971 *J. Phys. C: Solid State Phys.* **4** 1091
[12] Jiang Y and Gou C 1992 *Int. J. Mod. Phys.* B **6** 3279
[13] Comès R and Shirane G 1972 *Phys. Rev.* B **5** 1886
[14] Currat R, Comès R, Dorner B and Wiesendanger E 1974 *J. Phys. C: Solid State Phys.* **7** 2521